48TH TURBOMACHINERY & 35TH PUMP SYMPOSIA
HOUSTON, TEXAS | SEPTEMBER 9-12, 2019
GEORGE R. BROWN CONVENTION CENTER

EXPERIMENTAL EVALUATION OF PERFORMANCE AND MECHANICAL RELIABILITY FOR HIGH PRESSURE CO2 INTEGRALLY GEARED COMPRESSOR

Toshiaki Baba
Senior Engineering Manager
Kobe Steel, Ltd.
Takasago-city, Hyogo, Japan

Hirotoshi Arihara
Senior Researcher
Kobe Steel, Ltd.
Kobe-city, Hyogo, Japan

Shunsuke Morinaka
Researcher
Kobe Steel, Ltd.
Kobe-city, Hyogo, Japan

Takuya Iwata
R&D Engineer
Kobe Steel, Ltd.
Takasago-city, Hyogo, Japan

Koumei Fujioka
Mechanical Design Engineer
Kobe Steel, Ltd.
Takasago-city, Hyogo, Japan

Yoshitaka Baba
Deputy General Manager
Kobe Steel, Ltd.
Takasago-city, Hyogo, Japan

Yuki Kameyama
R&D Engineer
Kobe Steel, Ltd.
Takasago-city, Hyogo, Japan

Toshiaki Baba is a Senior Engineering Manager of Turbo Compressor Section in the Rotating Machinery Engineering Department for the Machinery & Engineering Company of Kobe Steel, Ltd. (KOBELCO), in Takasago, Japan. He worked as a fluid machinery researcher for 10 years and as a mechanical and electric engineer of electric power supply for 10 years. He has been involved in engineering and product development works for centrifugal compressors for over 10 years.
His current duties are mainly focused on detailed engineering and development of centrifugal compressors.
Mr. Baba has a BS and MS degree in Mechanical Engineering from Kyoto University.

Koumei Fujioka is a Mechanical Design Engineer of Turbo Compressor Section in the Rotating Machinery Engineering Department for the Machinery & Engineering Company of Kobe Steel, Ltd. (KOBELCO), in Takasago, Japan. He has been involved in engineering and product development works for centrifugal compressors since 2010. His current duties are mainly focused on detailed engineering of centrifugal compressors.
Mr. Fujioka has a BS and MS degree in Mechanical Engineering from Hiroshima University.

Hirotoshi Arihara is a Senior Researcher of the Dynamics & Acoustics Research Section for the Mechanical Engineering Research Laboratory of the Technical Development Group of Kobe Steel, Ltd. (KOBELCO), in Kobe, Japan. He is a specialist of rotor dynamics, hydrodynamic bearings and mechanical vibration. He has 9 years of experience with research of centrifugal compressors, screw compressors, and other industrial machinery.
Mr. Arihara has a MS degree in Mechanical Engineering from Tokyo Institute of Technology.

Yoshitaka Baba is a Deputy General Manager of the Technical Development Department for the Development Center of the Machinery Business Sector of Kobe Steel, Ltd. (KOBELCO), in Takasago, Japan. He is a specialist of rotor dynamics, hydrodynamic bearings and mechanical vibration. He has over 25 years of experience in research and development of centrifugal compressors, radial expanders, and other industrial machinery.
Mr. Baba has a BS and MS degree in Mechanical Engineering from Tohoku University.

Shunsuke Morinaka is a Resercher of the Dynamics & Acoustics Research Section for the Mechanical Engineering Research Laboratory of the Technical Development Group of Kobe Steel, Ltd. (KOBELCO), in Kobe, Japan. He is a specialist of dynamics and performance of labyrinth seals. He has 6 years of experience with research of dynamic and static performance evaluation about labyrinth seals for turbo compressors.
Mr. Morinaka has a BS and MS degree in Mechanical Engineering from Kyushu University.

Yuki Kameyama is a R&D Engineer for the Technical Development Department in the Development Center for the Machinery Business Sector of Kobe Steel, Ltd. (KOBELCO), in Takasago, Japan. He joined KOBELCO in 2010. He has been involved in analytical and experimental works for rotordynamics of turbomachinery since 2010. His current duties are mainly focused on rotordynamics and fluid filim bearing of centrifugal compressors.
Mr. Kameyama has a MS degree in Mechanical Enginnering from Tsukuba University.

Takuya Iwata is a R&D Engineer for the Technical Development Department in the Development Center for the Machinery Business Sector of Kobe Steel, Ltd. (KOBELCO), in Takasago, Japan. He joined KOBELCO in 2008. He has been involved in both analytical and experimental works for turbomachinery since 2008. His current duties are mainly focused on aerodynamic and rotordynamic design and testing of centrifugal compressors.
Mr. Iwata has a MS degree in Mechanical Engineering from Kyoto University.

ABSTRACT

Energy saving has become a trend as well as a countermeasure for global environmental issues. It can be one of the efficient solutions for reducing energy consumptions by adopting integrally geared compressors instead of inline compressors for industrial plants. It is possible to select the optimized rotating speeds for each pinion of compressor, resulting in improved stage efficiency. Inter coolers can be easily implemented for each stage, contributing to the reduction of the total power consumption. The development of key technologies for the design centrifugal compressor such as CFD, FEM, Rotor dynamic Analysis, Sealing etc., has enabled integrally geared centrifugal compressors for higher pressure applications than ever.
A commercial size, 5 stages integrally geared CO2 centrifugal compressor of 2900psiG / 20MPaG discharge pressure level was designed, manufactured and evaluated the fluid dynamic performances and rotor stability. It was installed in OEM's factory and the full load and full pressure test was carried out using real CO2 gas. The actual compressor fluid dynamic performance has shown superior results even at high pressure supercritical gas conditions at the high pressure stages of the compressor. The mechanical performances such as rotor vibration and bearing temperature were also measured and observed that the vibration was substantially

low and within safe limits even at high pressure operating conditions above 2900psiG / 20MPaG.
The authors conducted not only above mentioned basic measurements but also state-of-the-art special tests, i.e., (i) To check if the rotor dynamics is suitable for practical operations in industrial plant. (ii) To analyze the strength of impeller blade. Also the authors established a novel on Direct Rotor Excitation Method to experimentally investigate the rotor stability even at a high operating pressure level of 2900psiG / 20MPaG. With this technique the measurements of the actual rotor natural frequencies and the damping ratios (log decrement) during high pressure operating conditions provided more precise results rather than conventional casing excitation method. Moreover, the test results clarifies that the measured natural frequencies are in a quite good agreement with the calculation and also the measured damping ratios of the rotor forward modes are higher than that of calculated values. The effects of increasing damping methods were also experimentally and analytically investigated during this test, namely squeeze film damper bearings. The open impeller blade vibration was measured during running condition by using a non-contact blade vibration measurement technique. This measurement results revealed that impeller blades stress against the centrifugal force and the external excitation force was very low compared to the allowable stress value of the impeller material. It is also important to know the actual thrust force acting on the high speed shafts especially for high pressure compressors to ensure a reliable operation. Thrust force was directly measured during operation by implementing a strain gauge in thrust bearings of high speed shafts. Acquired data have verified that the thrust bearing design is appropriate. The fluid dynamic characteristics and mechanical reliability are assessed as acceptable including super critical gas condition of CO2 gas.

INTRODUCTION

The integrally geared compressors and inline compressors are widely used across the globe. Higher efficiency can be expected in the former since the optimal operating speed is designed for each stage (pinion), which leads to reduced energy consumption. Intercooler implementation is simpler than in the latter and reduces the total energy amount. Figure 1 shows compression diagram of integrally geared compressor and inline compressor. In this case, six inter coolers are equipped for integrally geared compressor, while three coolers for inline compressor. Temperature rise is suppressed in the former thus power consumption becomes smaller than in the latter. There are several key technologies such as (i) Rotor dynamic design (ii) High pressure casing design (iii) high pressure gas seal (iv) Aerodynamic component design for high pressure ~~condition~~ operation including super critical area and (v) Impeller blade strength design., which has to be implemented in order to employ integrally geared compressors for high pressure gas compression usage, such as Carbon Capture and Storage (CCS), Urea plant and S-CO2 Power Cycle (Bennett et al 2017). The progress of these technologies is nowadays remarkable and enables integrally geared compressors to get into high pressure applications more than 2900psiG / 20MPaG. The authors designed, manufactured and tested the integrally geared compressor at full pressure - full load conditions with CO2 gas using above mentioned technologies. The result verified aerodynamic and mechanical performances as expected. A schematic evolution of this development project is drawn in Figure 2. In addition to the usual measurements, newly developed methods were also applied and the authors succeeded in capturing running rotor conditions, such as natural frequency and log decrement, impeller blade stress and thrust force on bearings during high pressure operation. These are usually not easy to measure but expected to be quantitatively verified for safety operation. The measured log decrement has shown higher value than calculated. The blade stress and thrust force measurements is under safe limits with enough margin from designed allowable valve. All these verified results qualifies our integrally geared compressor design and it is suitable for high pressure gas compression applications with reliable confidence.

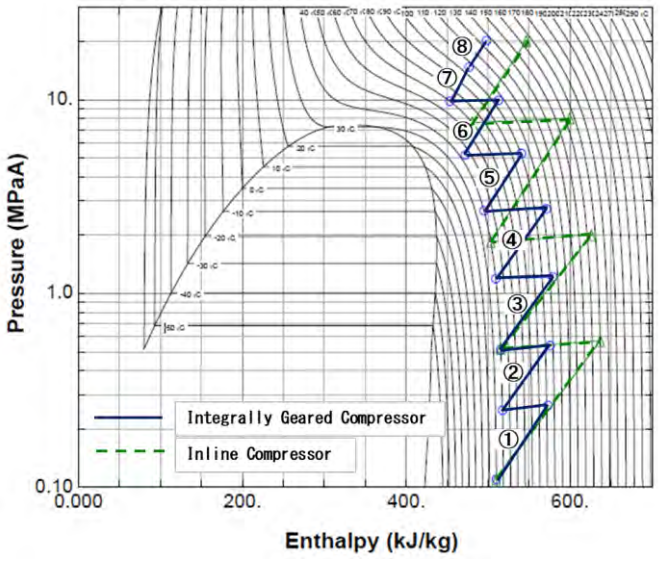

Figure 1: Compression diagram

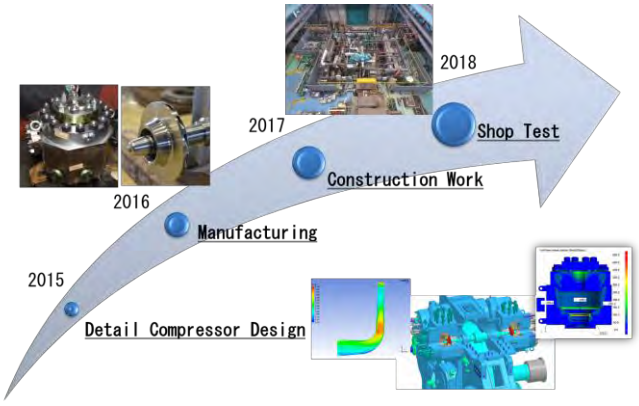

Figure 2: Evolution of Experimental Evaluation

DESIGN AND MANUFACTURING OF PROTOTYPE COMPRESSOR

Overview of prototype compressor and test apparatus

Testing an actual size compressor at full pressure and full load condition using real gas is the best way to determine the performance. Miniature models are sometime used but it is not always sufficient to verify the reliability in actual use (Metz et al 2015). For example, in a miniature model it is not possible to simulate the rotor behavior because all geometrical shapes cannot be proportionally reduced. Therefore, the vibration and damping measurements in an actual machine will always be different from a miniature model. Hence, the authors decided to design, manufacture and test the actual size compressor as a prototype to eliminate any unknown or uncertain factors related to size.

A relatively large CO2 compressor was selected as a prototype, which covers CCS application and large size Urea plant application (Musardo et al 2012). The specifications of the compressor are listed in Table 1 in comparison with ones of typical CO2 compressor for Urea application.

Basically, eight compression stages are required to develop a discharge pressure of 2900psiG / 20MpaG from atmospheric pressure. Therefore, the authors designed all eight stages at first and validated the design by confirming the dimensions of all parts, interference between the parts, piping accessibility for maintenance

Table 1: High Pressure CO2 Compressor Specification

Application	Prototype	Urea Application (1000 ～ 3300mtpd)
Type	Integrally Geared	Integrally Geared
No. of stage	8 Stages	8 Stages
Gas handled	CO2	CO2
Capacity	140,000 kg/hr (72,500 m3/hr)	up to 110,000 kg/h (57,000 m3/hr)
Suction/Discharge Pressure	0.01 / 20 MPaG	0.01/16 MPaG
Shaft Power	16,600 kW	up to 13,000 kW
Driver	Sync. Motor (18,500kW)	Motor/ Steam Turbine

Table 2: Prototype CO2 Compressor Specification

Type	Integrally Geared
No. of stage	5 stages High Pressure parts
Gas handled	CO2
Capacity	140,000 kg/hr (6,700 m3/hr)
Suction/Discharge Pressure	1.0 / 20 MPaG
Shaft Power	8085 kW
Driver	Shop Motor

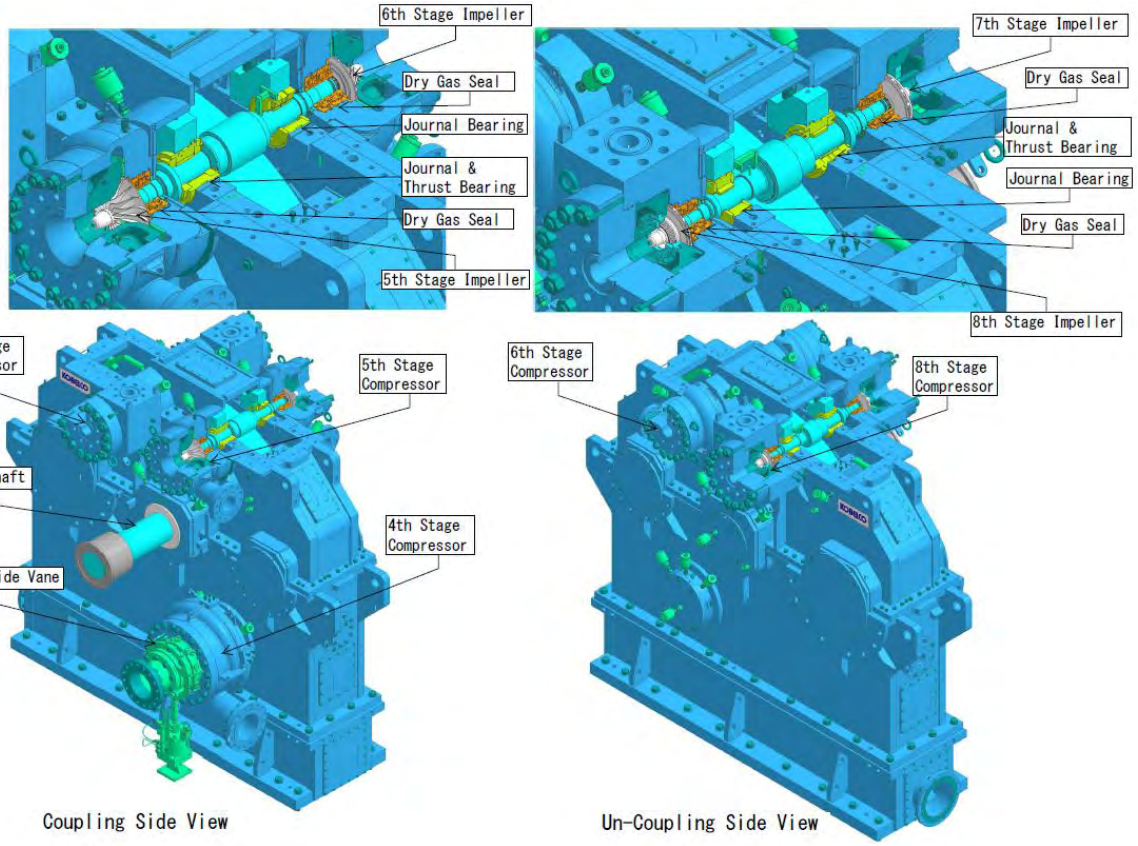

Figure 3: External Look of Integrally Geared Centrifugal Compressor (Prototype Machine)

and so on. Since, the low pressure stages (1st stage to 3rd stage) has no any special technical factors to be tested or measured during actual operation, only the high pressure stages (4th stage to 8th stage) were manufactured and tested. OEM had a lot of experience for such low pressure compression. The suction pressure of 145psiG / 1.0MPaG was adopted for the 4th stage instead of atmospheric pressure. This suction pressure corresponds to the same pressure of the 4th stage suction in the 8-stage compressor specified in Table 1.The prototype machine consists of a total five stages namely 4th, 5th, 6th, 7th and 8th, which represents more severe conditions than the low pressure part. The specification of the compressor tested is shown in Table 2.

Open impellers are adopted for 4th stage to 6th stage whereas covered impellers for 7th and 8th stage. All the impellers are specially designed for the test considering the characteristics of carbon dioxide gas. The external look and the internal configuration of the main parts are described in Figure 3. The integral gears of the prototype compressor consist of one bull gear rotor and three pinion rotors. All pinion rotors are supported by tilting pad journal bearings. Squeeze film damping function is equipped for 5th, 6th, 7th and 8th stage rotor journal bearings to ensure high rotor stability. Thrust bearings are implemented to support thrust forces applied on each pinion shaft. Tandem dry gas seals are used for shaft sealing of all high pressure stages (4th stage to 8th stage). The cross section drawing for 5th stage to 8th stage is show in Figure 4.

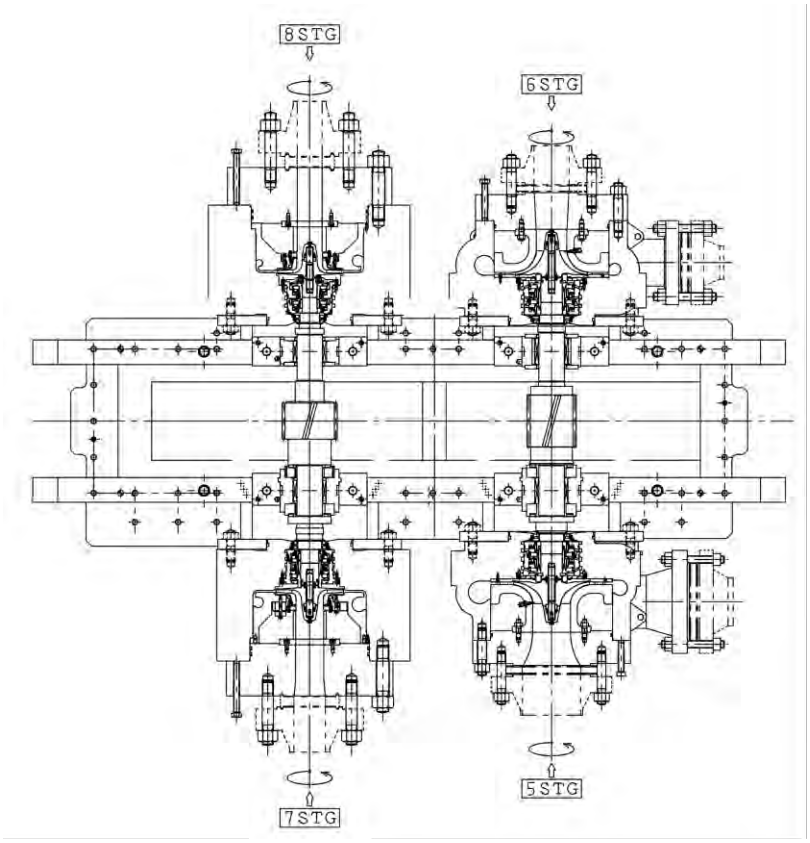

Figure 4: Cross section drawing for 5th to 8th Stage

The dynamic balancing and over speed tests for impellers were performed before assembling the rotor. An input shaft with bull gear is connected to a shop motor via a flexible coupling. Compressor casings (all stages) are specially designed and manufactured to withstand the maximum operating discharge pressure. All the casings will go through hydrostatic test and leakage test before being introduced to operational test. An inlet guide vane is installed at the upstream of 4th stage and it adjusts the flowrate through the compressor. The location and the number of the inlet guide vanes might be different from this configuration in a full 8 stage compressor depend on the system requirement, however it is enough just to adjust total flowrate for the test of this unit.

A closed loop is designed for the test and inter coolers are installed between the 4th and 5th stage, 5th and 6th stage, 6th and 7th stage respectively. A main bypass cooler is equipped across 4th stage suction and 8th stage discharge. The main bypass valve in this loop regulates the discharge pressure. Intermediate bypass line is also connected between the 5th discharge and the 4th suction line enabling startup and relatively low pressure operation. Carbon dioxide gas is fed into the 4th suction line of the closed loop system from CO2 supply source at test shop. The schematic representation of the test loop and over-view of the test bench are shown in Figure 5 and 6, respectively.

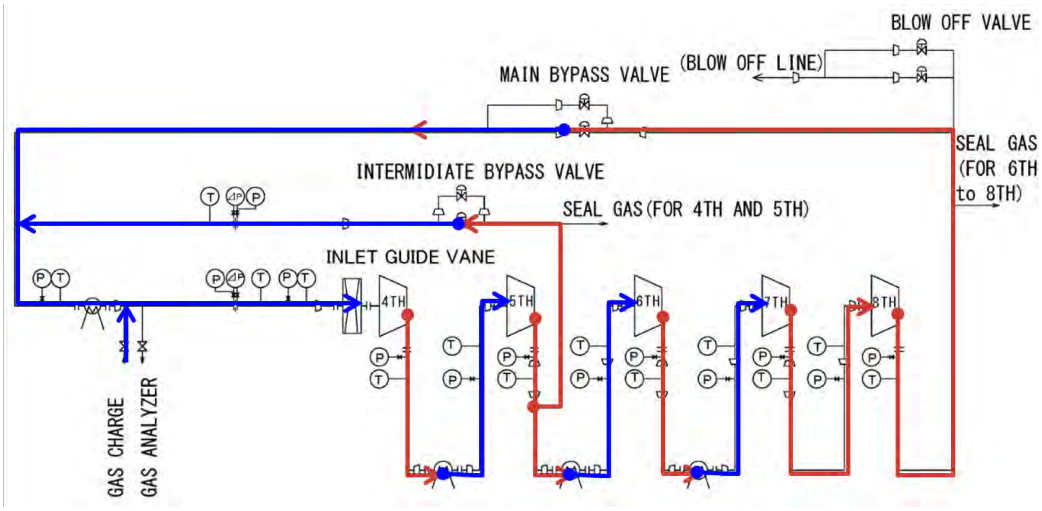

Figure 5: Process Flow Diagram of The Prototype Compressor

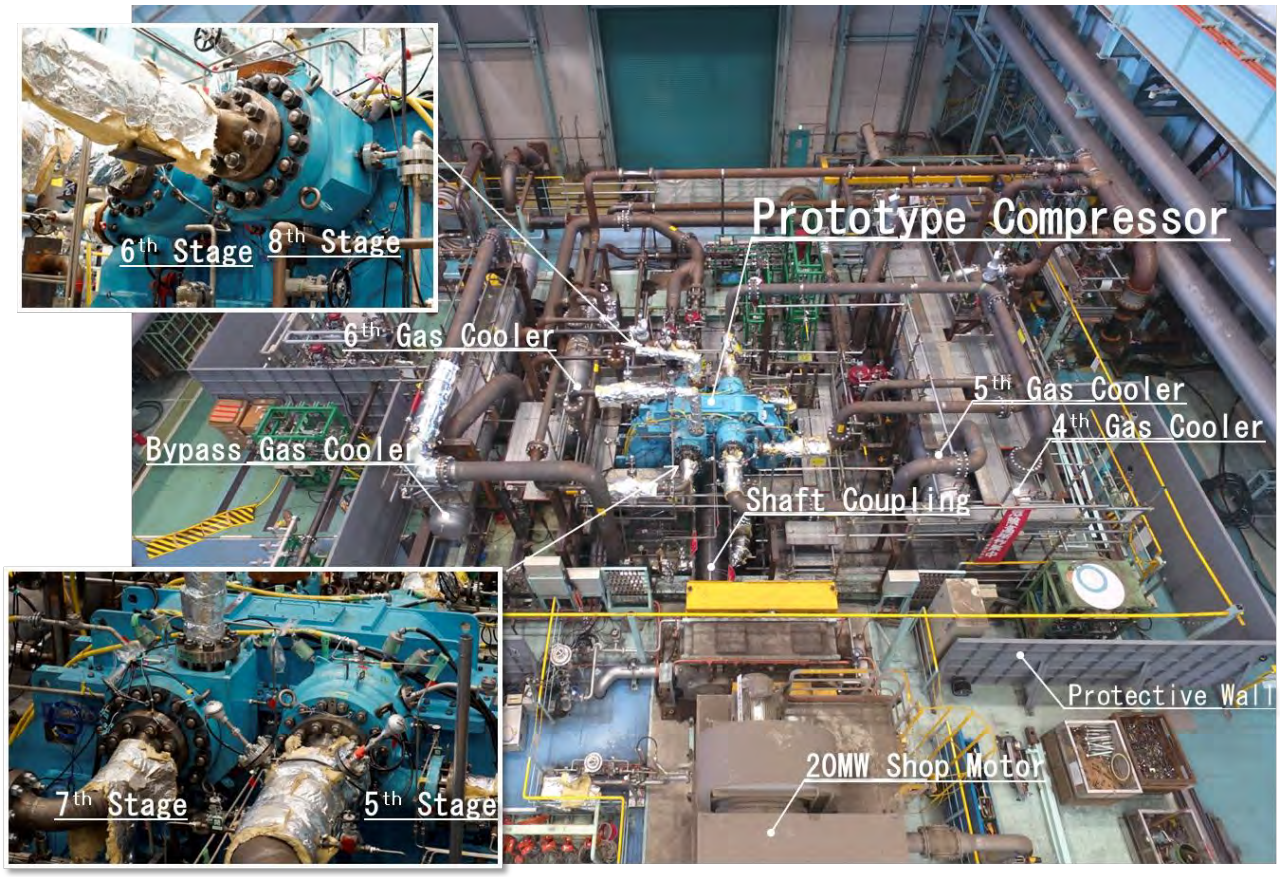

Figure 6: Overview of the Prototype Compressor and Test Facility

Main component design and test

Compressor casings for all five stages were designed and FEM analyzed, since higher stress was expected than that of usual compressors because of high pressure. As a result of stress concentration, a relatively higher stress than yield strength of the material was revealed near the tongue area of the scroll casing by FEM. Elasto-plastic analysis was carried out to assess the stress by using material characteristics data obtained from the test piece of same material. The analysis results were assessed according to ASME Section VIII and concluded that the designed casing had enough fatigue strength against expected usage for over 20 to 30 years as an industrial compressor. Not only FEM analysis but also actual stress was evaluated by means of strain gauges during pressurized test of the casing to verify FEM calculation results. Figure 7 displays the comparison of FEM analysis with actual stress measurements at the center of casing flow passage and confirmed that the casing design is within the permissible stress limits.

Figure 7: FEM Analysis and Strain Measurement of Compressor Casing

Rotor design was a key factor to enable a stable operation. The API regulates minimum log decrement for external excitation force on the rotor. Since the average gas density was relatively high, Level II stability analysis was required for rotors of 5th to 6th stage and 7th to 8th stage. The dynamic effects from impeller and seals that contribute to the overall stability of rotating assembly were examined and included in the analysis. The original rotor design could not satisfy the regulation because of stronger destabilizing fluid force acting on impellers of 7th to 8th stage rotor. Therefore, swirl brakes were implemented in front of the impellers, due to which the minimum criteria had passed (L. Baldassarre et al. 2014), however, still further stability was ~~still~~ desired. Followed by the installation of squeeze film dampers to the journal bearings and then log decrement had finally improved sufficiently high as expressed in Figure 8 and 9. Since it was considered that the measurement of rotor vibration during operational test is not sufficient, a special measurement was adopted to obtain the rotor natural frequency and log decrement during running condition by implementing additional design to the compressor. Details and test results are described in the latter section.

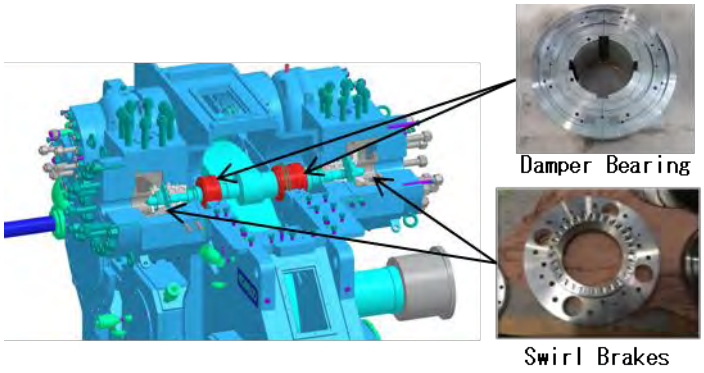

Figure 8: Components for Rotor Stability

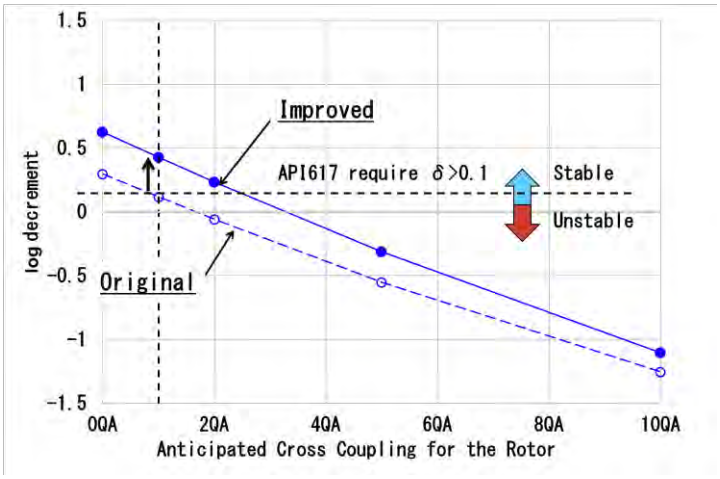

Figure 9: Improvement of Rotor Stability

Covered impellers were adopted for 7th and 8th stage, where the gas pressure is high and their blade heights at the exit are very small. The gas condition is in supercritical region and thus special care about CO2 gas property should be paid to the design of impeller blades. Computational fluid dynamics was performed to study the velocity distribution through the impeller blades with CO2 gas properties. As a result of this study, the blade passage was optimized from conventional design to attain a smooth velocity distribution. The conventional design shows the existence of two velocity peak areas in the blade passage (upper left in Figure 10), whereas the velocity peak area had reduced in the optimized blade passage (upper right in Figure 10) and it was expected to have smooth velocity change. The gas flow around the impeller seal at the suction part was also investigated and modified to reduce the leakage flow rate by implementing step and front seal, thereby reducing the leakage amount by about 35 percent (lower in Figure 10). The impeller efficiency was increased by a few percent in total.

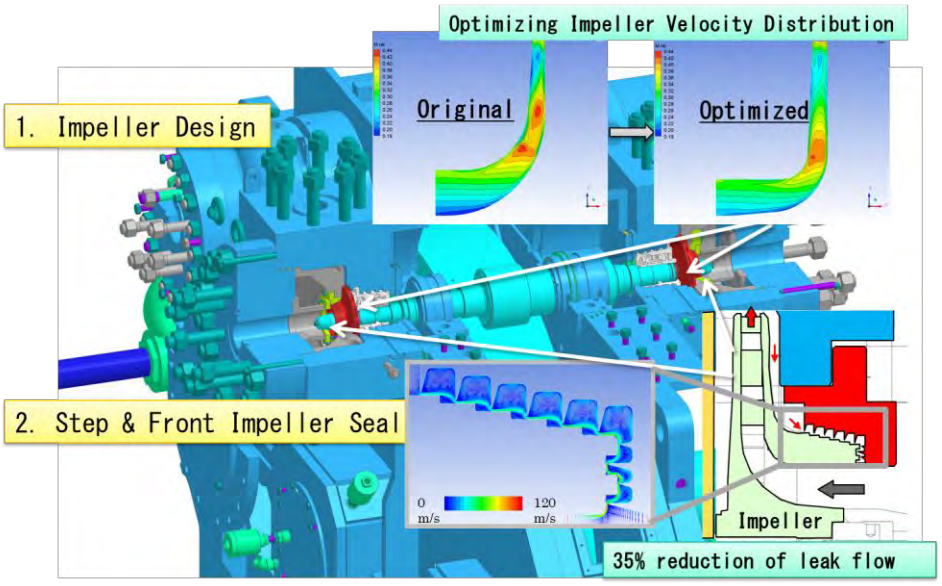

Figure 10: Optimization of Impeller and Seal

In order to apply an integrally geared compressor to high pressure gas compression applications, a gas seal has a quite important role. Generally gas seal in an integrally geared compressor has to withstand higher pressure difference than that of an inline compressor. A dry gas seal of seal size 2 inch / 51 mm, was selected for this prototype compressor to seal CO2 gas between 3600psiG / 25MPaG and

atmospheric pressure. The improved dry gas seal technology has enabled sealing against such high pressure difference even at a high rotational speed say 20,000 rpm for this integrally geared compressor. Prior to implementing a dry gas seal into the prototype compressor, a seal performance test with running condition and at a pressure level of 2900psiG / 20MPaG has been conducted as a component test using real gas (CO2) at dry gas seal manufacturer`s shop. The test results had shown a far superior sealing performance than expected. Since it is rare to measure the seal leakage flowrate during actual operation, this adopted measurement method was decided to be applied as one of special measurements for a prototype compressor testing especially for the last stage (8th stage), where the pressure level was the highest. The specification of dry gas seals is mentioned in Table 3.

Table 3: Dry Gas Seal Specification

Stage	5th	6th	7th	8th
Shaft Diamter	75 mm	75 mm	63 mm	51 mm
Rotational Speed	18387 rpm		16286 rpm	
Gas	CO2			
Pressure	3.6 MPaG	7.7 MPaG	13.3 MPaG	18.3 MPaG
Temperature	95°C	65°C	100°C	100°C
Expected Leakage	18 Nl/min	55 Nl/min	45 Nl/min	74 Nl/min

FULL PRESSURE AND FULL LOAD TEST

The prototype compressor was installed at OEM's test bench as shown in Figure 5, and the operational test was performed with CO2 gas. The test started at relatively low pressure condition and the mechanical and aerodynamic performances were monitored. The gas pressure level was gradually increased step by step until it finally reached the rated pressure level of 2900psiG / 20 MPaG. The main purposes of this test is 1) to measure static performance and 2) to verify usually unknown values. The former includes aerodynamic performance of each stage and mechanical performance such as rotor vibration and bearing temperature. These are usually measured at site to detect any abnormal conditions. However, it is difficult to determine the performance margin from the design criteria at site by simply monitoring trend data. Knowing how much margin is left makes it possible to give confidence to stable operation and verify proper design. The latter purpose is to come up with such expectation. Following special and state-of-the-art measurements were planned and carried out in this full pressure and full load test. They are a) rotor natural frequency and log decrement measurement, b) impeller blade vibration and stress measurement and c) thrust force measurement. All of them were performed during operation without affecting the original compressor performance and succeeded in generating quite meaningful and reasonable data. Details are described in the latter sections.

Mechanical performance

The mechanical performance test for shaft vibration and bearing temperature was carried out as first assessment, which is usually monitored to confirm stable operation. Two vibration sensors were equipped at each stage and continuously measured during the test. Lubrication oil was supplied at a required operating pressure and confirmed that the oil flowrate was within the desired value. All shaft vibrations were below API 617 criteria even at high discharge pressure condition i.e. 2900psiG / 20MPaG as shown in Table 4. Bearing temperatures were also much lower than OEM's criteria for all stages. Based on these test results the mechanical design of the prototype compressor was judged suitable as a high pressure integrally geared centrifugal compressor. The bearing specification is summarized in Table 5.

Table 4: Mechanical Performance Test Results (Rated Condition)

	Result	Criteria	Judgement
Shaft Vibration	5th: 10um 6th: 15um 7th: 18um 8th: 19um	API 617 criteria 5th-6th: 21um 7th-8th :22um	OK
Journal Bearing Temperature	5th: 70°C 6th: 74°C 7th: 65°C 8th: 69°C	Equal and less than 105°C	OK
Thrust bearing Temperature	5th: 75°C 7th: 90°C	Equal and less than 105°C	OK

Table 5: Bearing Specification

Stage	5th	6th	7th	8th
Journal Bearing				
Type	Tilting Pad			
Shaft Diamter	88.9 mm	88.9 mm	88.9 mm	88.9 mm
Rotational Speed	18387 rpm		16286 rpm	
Oil Type	VG32			
Oil Temperature	43°C			
Thrust bearing				
Type	Tilting Pad	N.A.	Tilting Pad	N.A.
Pad Diamter	151.6 mm		145.3 mm	
Rotational Speed	18387 rpm		16286 rpm	
Oil Type	VG32		VG32	
Oil Temperature	43°C		43°C	

Improvement of mechanical stability

It is generally known that destabilizing fluid force applied on impeller and shaft increase when the gas pressure becomes high (Moore et al 2011). The shaft vibration was sudden increased when the gas flowrate was lower than the normal operating flow for original compressor design as shown in Figure 11. The vibration was detected at highest pressure stages i.e. 7th & 8th stage and it exceeded the allowable criteria for continuous operation. FFT analysis revealed that the cause of increased vibration was mainly due to sudden development of sub synchronous vibration around 60Hz. This frequency of 60Hz is corresponding to approximately 20 percent of the rotating speed. A similar phenomenon was studied for the high pressure compressor rotors, in which the rotating stall at the diffuser was considered as the fundamental cause especially for such high density gas compressors (Nishida et al 1991). The authors investigated this flow characteristic by Computational Fluid Analysis (CFD) and found the reverse flow area around the impeller exit in vaneless diffuser as shown in Figure 12. Analysis results suggested that the sub synchronous vibration was induced by the rotating stalls occurring immediately downstream of the impeller, although it was a steady state ~~the~~ analysis. The reverse flow was found near the impeller exit, which might affect main gas flow around this area. Vanned diffuser implementation was considered instead of vaneless diffuser as a countermeasure to suppress the rotating stall or the reverse flow and it was expected to reduce shaft vibration. The effects of the number of diffuser vane and the vane height were examined. A variety of number of diffuser vanes and diffuser height combinations were examined by CFD to find out the best combination, which made the area of the revers flow much narrower. As a result of above investigation, the vanned diffuser was optimized and fabricated (Figure 13). The vanned diffusers were implemented to 7th and 8th stage compressor casings and the operational test was carried out again with full pressure and full load condition. The shaft sub synchronous vibration around 60 Hz was successfully suppressed as expected at the small flowrate condition (Figure 14), which enabled to operate at smaller flow condition than the previous configuration using vane less diffusers.

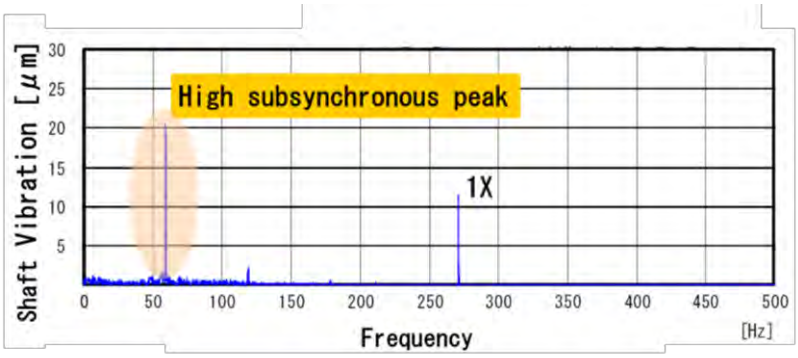

Figure 11: FFT Analysis of Shaft Vibration at 7th Stage (Original)

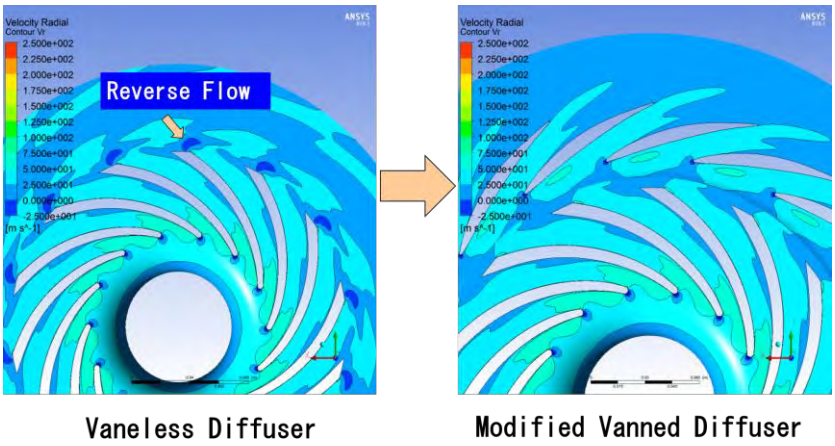

Figure 12: CFD Analysis at Small Flow Rate Condition

Figure 13: Diffuser Vane (8th Stage)

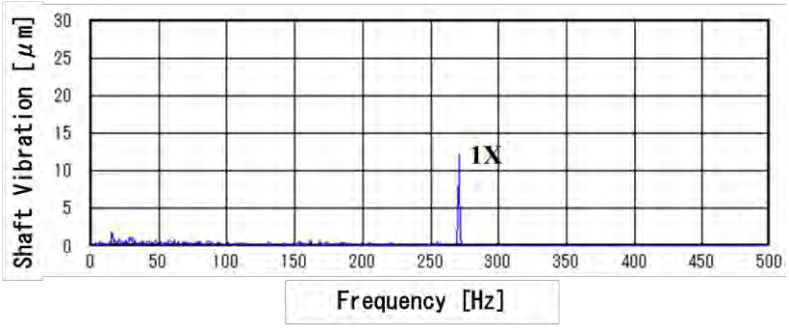

Figure 14: FFT Analysis of Shaft Vibration at 7th Stage (After Modification)

Aerodynamic performance

Gas pressures, temperatures and flowrates were measured at inlet and outlet of each stage of the prototype compressor to assess the aerodynamic performances. The inlet pressure of the 4th stage was kept constant by adjusting the supply and discharge pressure of CO2 gas and the flowrate was controlled by the discharge bypass valve. The flow coefficient versus the discharge pressure of the 5th to 8th stages is shown in Figure 15. The graph of flowrate is normalized by inlet volume flow of each stage. The rated discharge pressure of 2900psiG / 20MPaG was attained around the rated flow coefficient. Gas compression in supercritical zone is requested for especially the 7th and 8th compressor stages, where special design consideration was taken into account. Comparison between the expected performance and the actual test performance of the 8th stage is plotted in Figure 16, in which the test result shows higher Polytropic efficiency than expected, thus the appropriately designed aerodynamic parts including the impeller is appreciable. All of these are test results with diffuser vanes.

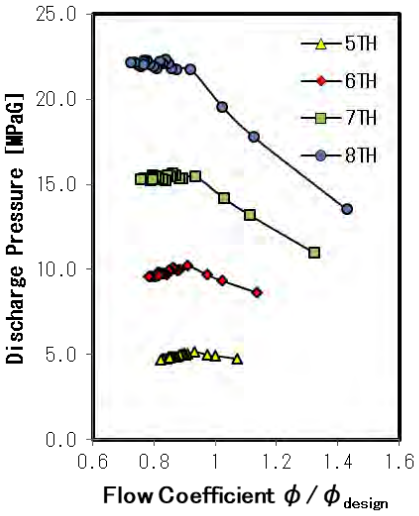

Figure 15: Discharge Pressure of Each Stage

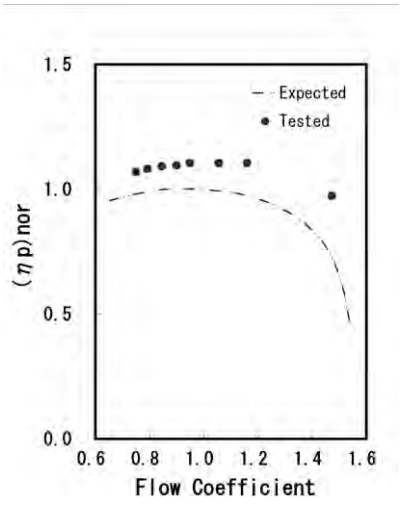

Figure 16: Polytropic Efficiency of 8th Stage

Dry Gas Seal leakage flowrate measurement

Gas seal is also quite an important factor to apply integrally geared compressors to high pressure compression usage, where the differential pressure across the seal is usually higher than that of inline compressors. The amount of leakage from 8th stage dry gas seal was measured during the operational test. The seal size is 2 inch / 51 mm and its maximum difference pressure is 3600psiG / 25MPaG. It was confirmed that the leakage amount was the same level as that of the dry gas seal shop test results acquired by the dry gas seal manufacturer, which was significantly lower than expected and guaranteed the value of the dry gas seal. The measured value was superimposed into the single test results shown in Figure 17.

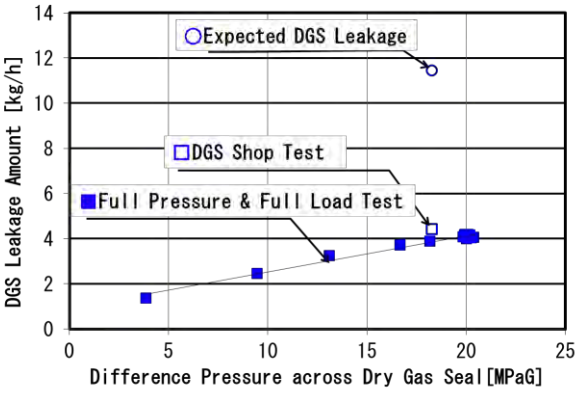

Figure 17: Dry Gas Seal Leakage Flow Measurement (8th Stage)

HIGH PRESSURE ROTOR STABILITY TEST

Justification of rotor stability evaluation

In high pressure compressors, the process gases become denser hence affecting the destabilizing fluid forces on the impellers. It is well-known that the high pressure fluid forces as well as the stiffness and damping of the bearings will greatly change the log decrement of rotors. In particular, the destabilizing fluid force decreases the log decrement of forward vibration modes. Once a negative log decrement occurs because of inappropriate rotordynamic design, such a rotor condition might cause serious unstable shaft vibration (Kulhanek et al. 2017). The API standard requires more than 0.1 rotor log decrement. Therefore, sufficiently high damping rotor dynamic design and the comprehensive stability test are very important to ensure the machine reliability under high pressure operation (Vannini et al. 2017).

If compressor OEMs can measure the log decrement of actual operating rotor, the mechanical reliability against unstable vibration will be demonstrated. A rotor log decrement measurement has to be performed under actual operating condition, because it highly depends on the operating load, i.e., discharge pressure and rotational speed. Generally, it is difficult to evaluate the rotor log decrement from steady operating vibration measurement, thus some OEMs attempt shaking test to excite the rotor vibration modes and observe the shaft vibration response by proximity probe. Since the excited vibration responses shaking from the outside of the casing are relatively small, further effective excitation method is desired for the rotor inside the casing.

The API standard exemplifies the rotor excitation method using the magnetic bearings. Research in the past has established a stability test sequence applying the magnetic bearings for the inline centrifugal compressors (Noronha et al. 2014, Vannini et al. 2014). However, most integrally geared compressors have no extra space for installing the magnetic bearings on the rotor, because there are a lot of components on the rotor, i.e., shaft seals, bearings, impellers and a gear mesh. However, extending the length of the rotor to place magnetic bearings will change the rotor shape, hence it is not an actual rotor design verification. According to above discussions, it is difficult to apply the magnetic bearings to the integrally geared compressors to evaluate rotor stability. In this paper, the authors have developed a novel direct rotor excitation technique using the magnetic exciters designed in-house. The development of compact magnetic exciters enables to be incorporated into the casing and can be an effective method of exciting rotor vibration modes.

Rotor excitation system configuration and principle

Figure 18 illustrates the excitation system developed. Four magnetic exciters are installed facing the 7th stage impeller shroud cover in the circumferential direction. The magnets are disposed outside the impeller to generate a bending moment that excites the rotor vibration mode though the generated forces acting in the axial direction of the rotor. The rotor has two rotating directions of vibration mode, one is along the rotational direction and the other is in the opposite direction.

The authors implemented a rotational excitation method to excite each directional mode independently based on phase controlled magnet currents. The excitation in the rotating direction is called forward rotational excitation, and the excitation in the opposite direction is called backward rotational excitation, respectively.

According to computational modal analysis, the authors verified that it is sufficient to install a magnetic exciter only to the 7th stage impeller for rotor stability evaluation. This rotor has totally four proximity probes, two each at 7th stage and 8th stage respectively which is commonly utilized near the journal bearings in X-Y direction to monitor shaft vibration. These probes will detect the shaft vibrations generated by magnetic excitation technique.

Figure 19 depicts a magnetic excitation system configuration and signal cable connections at the time of actual stability test. The magnetic exciters and the proximity probes are set inside of the compressor. The amplifiers to drive magnets are located near the test machine, the signal cables are wired to the control room and signals are acquired by data loggers.

In-house software generates an excitation command from PC #2 and signal generator outputs an excitation signal that passes through the amplifier to drive a magnet. The thermocouples are installed to each magnet to monitor coil temperatures to avoid overheating the coil due to applied current during excitation. And the data logger also collects the applied voltage and current to observe the actuation of magnets.

Figure 20 displays a cross sectional view of the magnetic exciters setup. The magnets are mounted in the compressor casing, making it possible to measure the rotor stability without affecting the rotor design. Figure 21 shows the mounted magnet assembly at the 7th stage impeller.

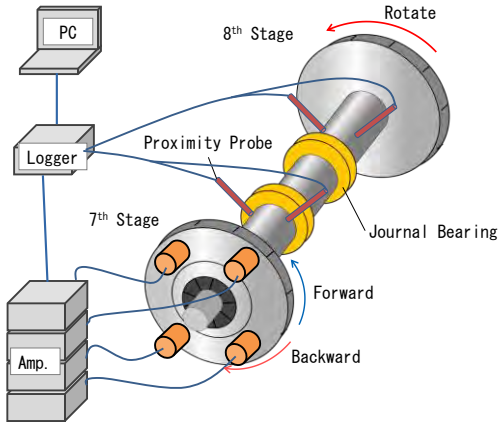

Figure 18: Principle of Developed Magnetic Rotor Excitation System

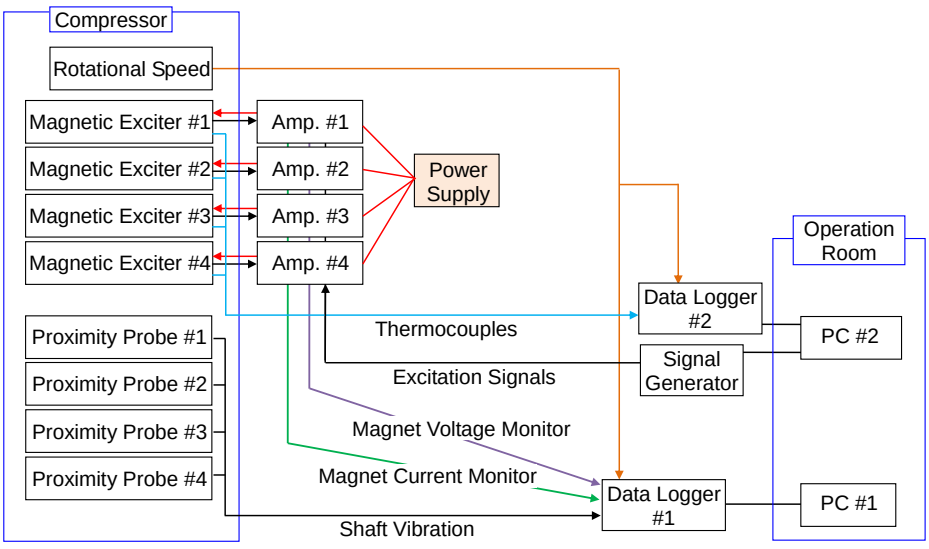

Figure 19: Magnetic Excitation System Configuration

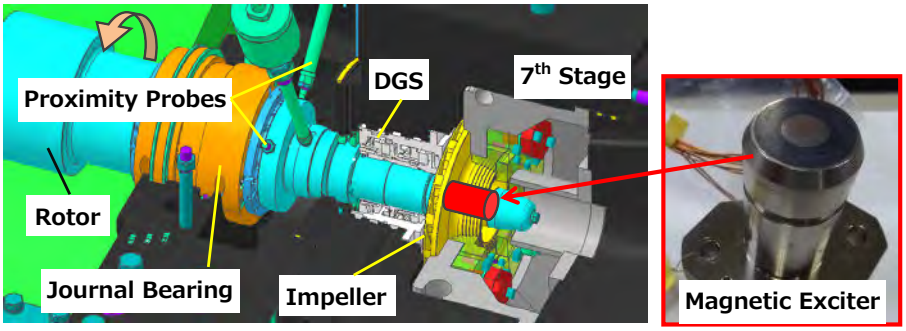

Figure 20: Cross Sectional View of the Magnetic Exciters Setup

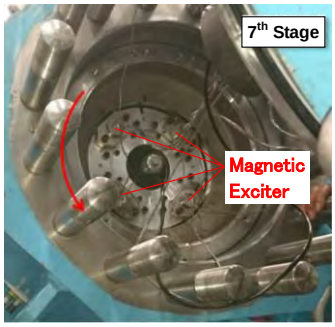

Figure 21: Magnet Assembly of 7th Stage Impeller

The specific measurement procedures are as follows:

- Output the swept sine excitation signals to drive magnets and measure the shaft vibration
- Perform FFT analysis for shaft vibration data to obtain frequency response functions (FRFs)
- Calculate directional FRFs (dFRFs) from the measured FRFs
- Apply curve-fit to dFRFs as experimental modal analysis to determine natural frequency and log decrement

The dFRFs are separate results of forward mode component and backward mode component included in FRF. It achieves more accurate modal analysis to obtain natural frequency and log decrement (Takahashi et al. 2007, Takahashi et al. 2011).
Figure 22 is a comparison of two dFRFs measured by proximity probes with and without excitation. The red line indicates background noise, the blue line renders rotor vibration response with excitation and the peak represents rotor natural frequency. A sharpness of a peak means a log decrement and a blunt peak suggests higher log decrement. The dFRFs with excitation denotes enough amplitude response and thus the magnetic excitation method proves to be effective. The conventionally applied method of stability test installs a shaker on the outside of casing to excite the vibration modes by external force (Tokuyama et al. 2014). This technique is however, difficult to directly excite the rotor vibration modes, thus reducing the measurement accuracy. Furthermore, it excites the unwanted casing vibration mode which is not subjected to rotor stability evaluation. Apparently, high pressure compressor casing has higher stiffness than low pressure casings, thus excitation of high pressure casing might measure insufficient vibration response.

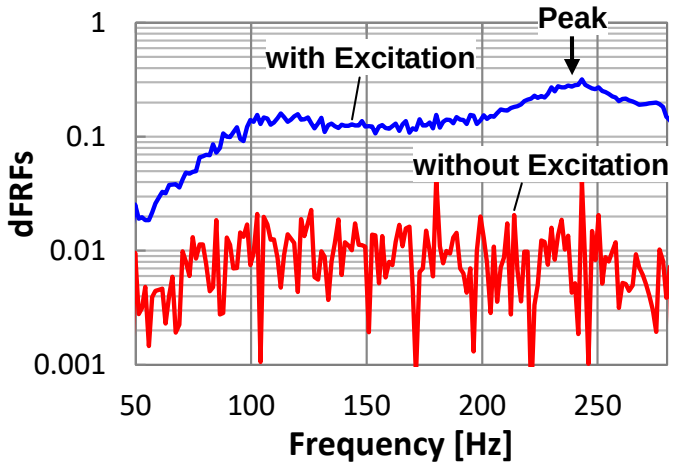

Figure 22: Comparison of dFRFs with and without Magnetic Excitation

Rotor excitation test result

Figures 23 and 24 show the FRFs measured by each proximity probe due to the excitation method developed on compressor under actual operating condition. The excitation frequency range of FRF is from 50Hz to 280Hz. Figures 25 and 26 show the dFRFs calculated from FRFs in Figures 23 and 24. Figure 25 shows dFRFs of backward excitation and Figure 26 shows dFRFs of forward excitation. Both shows clear peaks in the rotor vibration mode.
The curve fit of dFRFs can calculate natural frequency and log decrement. Figure 27 describes the magnitude and phase of measured dFRFs (blue line) with curve fit result (red line). The curve fit result identifies two forward modes in the excited frequency range and this result confirms the curve fit validity.

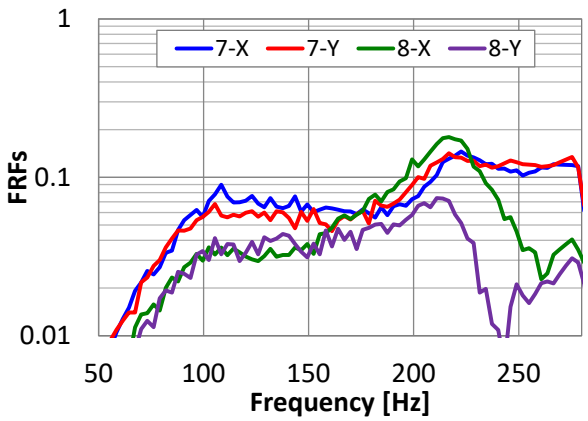

Figure 23: FRFs of Backward Excitation

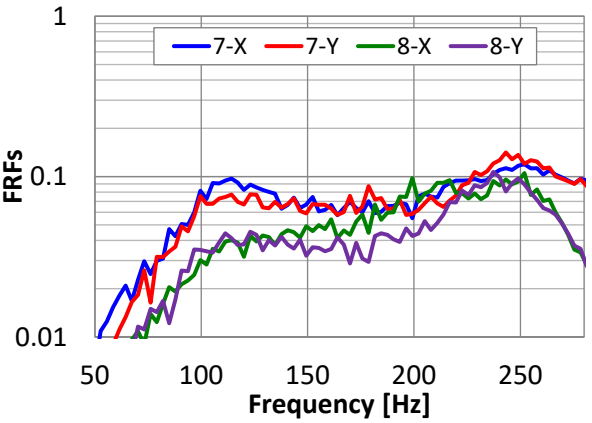

Figure 24: FRFs of Forward Excitation

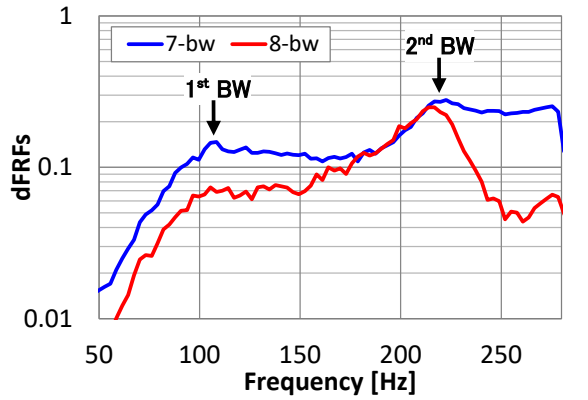

Figure 25: dFRFs of Backward Excitation

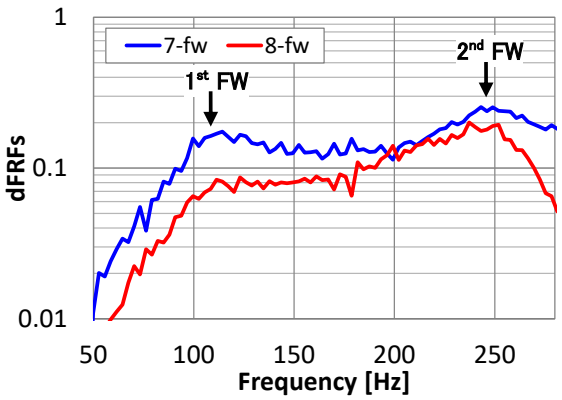

Figure 26: dFRFs of Forward Excitation

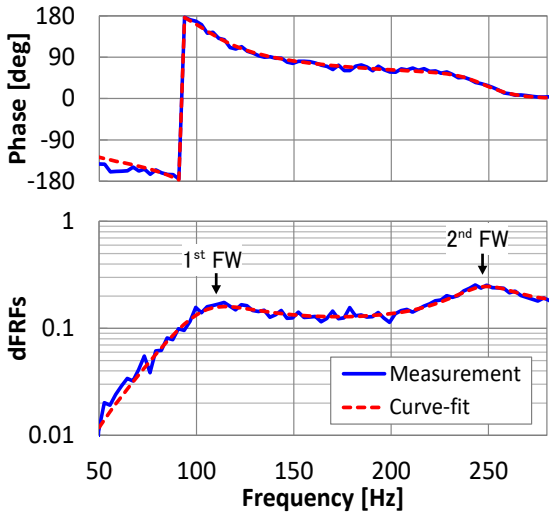

Figure 27: Curve Fit Results of Forward dFRF at Actual Operating Condition

Comparison of analysis results with test.

Figures 28 to 31 depict the rotor dynamic characteristics when operating at rated pressure of 2900psiG / 20MPaG. Figure 28 and 29 shows dynamic characteristics of rotor with tilting-pad journal bearing (TPJB). Whereas, Figures 30 and 31 shows TPJB with integral squeeze film damper (ISFD). Also, the natural frequency of forward mode is shown in Figure 28, the first mode is measured at 180Hz and the second at 250Hz, respectively. The predicted values are in good agreement with test results. Moreover, Figure 29 shows the measured log decrements are higher than the predicted ones which validates the safe design of rotor stability. These results quantitatively proved that the actual rotor log decrement is greater than 0.1 with enough stability margins.
Figure 30 also suggests good agreement with calculated natural frequencies and the measured values. In particular, the first forward

natural frequency (120Hz) of rotor with ISFD bearing is much lower than 180Hz compared with TPTJ (without ISFD) as shown in Figure 28. The calculated natural frequencies are close to the measured values, it proves the proper rotor design and prediction techniques of rotordynamics. In Figure 31, the calculated first forward mode log decrement well corresponds with the measured value. However, the measured second forward mode does not reach the predicted damping performance, although it sufficiently exceeds the requirements of API. These results clarifies that the rotor keeps enough stability under the rated pressure operation.

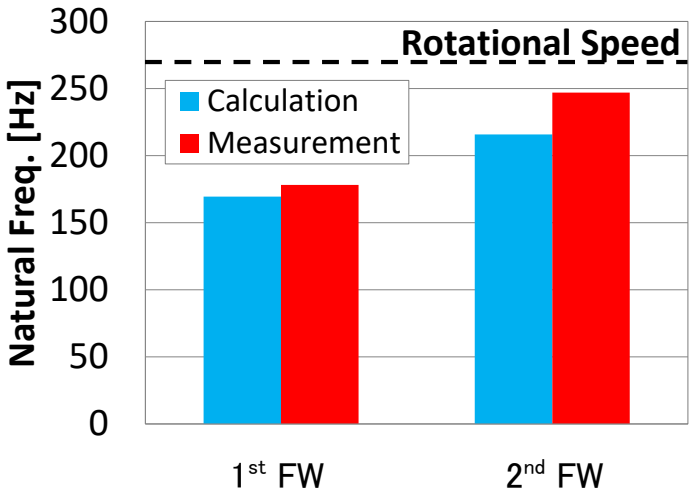

Figure 28: Dynamic Characteristics of Rotor with TPJB (Natural Frequency)

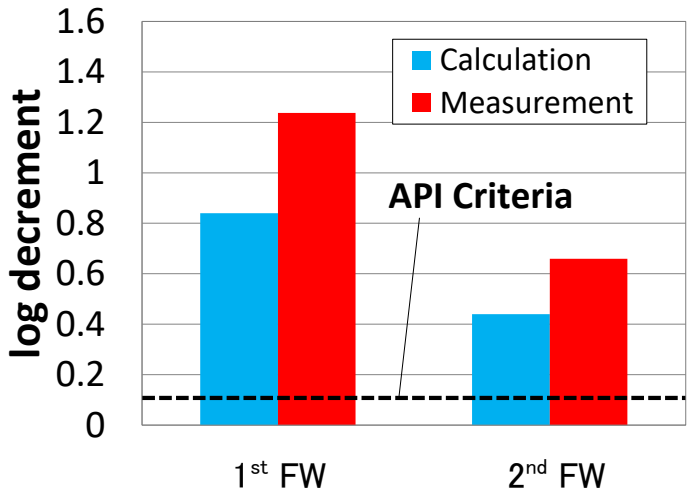

Figure 29: Dynamic Characteristics of Rotor with TPJB (log decrement)

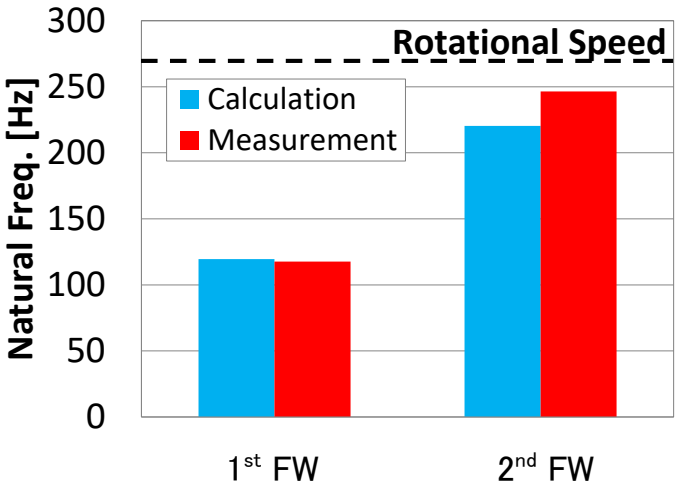

Figure 30: Dynamic Characteristics of Rotor ISFD Bearing (Natural Frequency)

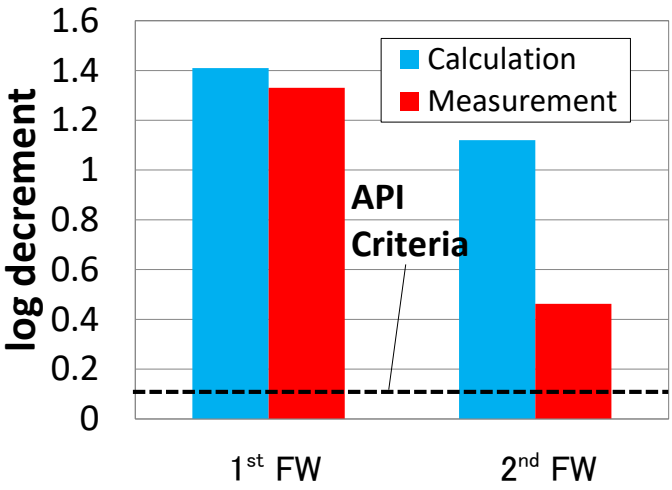

Figure 31: Dynamic Characteristics of Rotor ISFD Bearing (log decrement)

The operating pressure dependency of rotor dynamic characteristics

Figure 32 to 35 describes the behavior of measured rotor dynamic characteristics versus the change in discharge pressure. Figures 32 and 33 are for TPJB whereas Figures 34 and 35 are for the bearings with ISFD showing natural frequency and log decrement. As for natural frequency, it does not change significantly depending on the discharge pressure as shown in Figure 32, whereas the log decrements tends to decrease as the discharge pressure increases as shown in Figure 33. It still maintains much higher log decrement than 0.1 at a rated pressure of 2900psiG / 20MPaG. Figure 34 shows the rotor natural frequency in case of ISFD bearing, which indicates lower first mode natural frequency than that without ISFD case. In Figure 35, the second forward mode log decrement of ISFD somehow does not increase compared to TPJB. In addition, there is no deterioration of log decrements with increase in discharge pressure and keeps sufficient stability up to maximum discharge pressure. These results substantiate the validity of rotor stability design in this development.

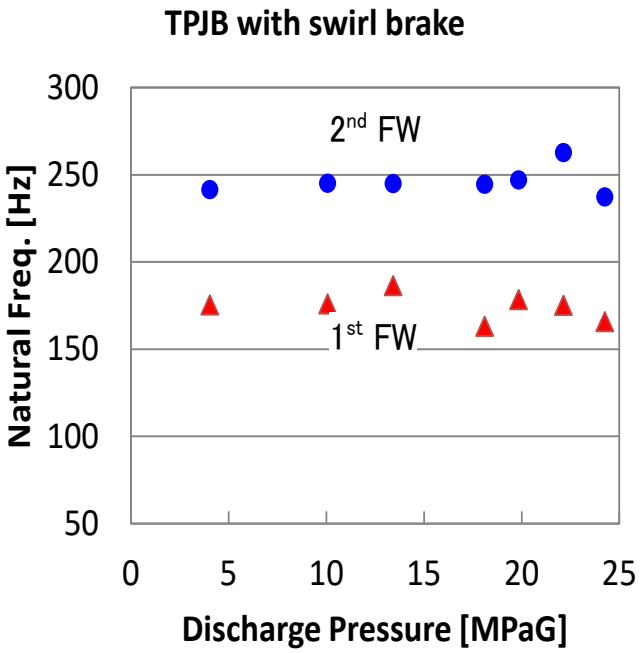

Figure 32: Measured Natural Frequency

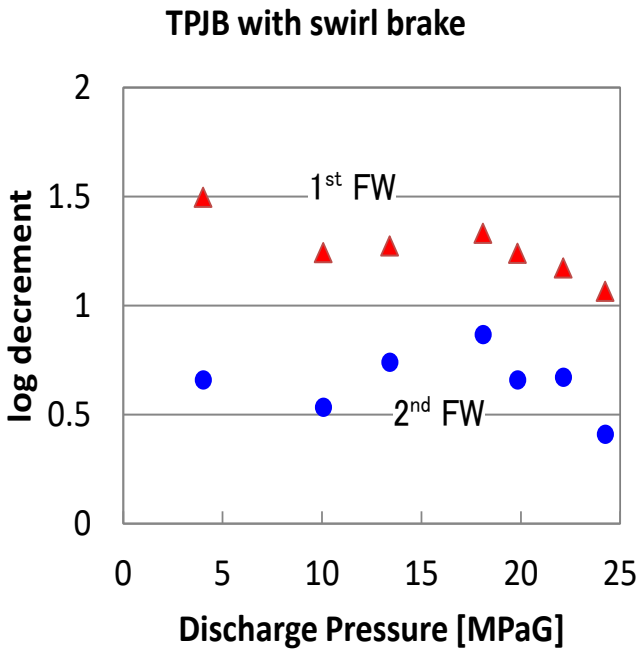

Figure 33: Measured log decrement

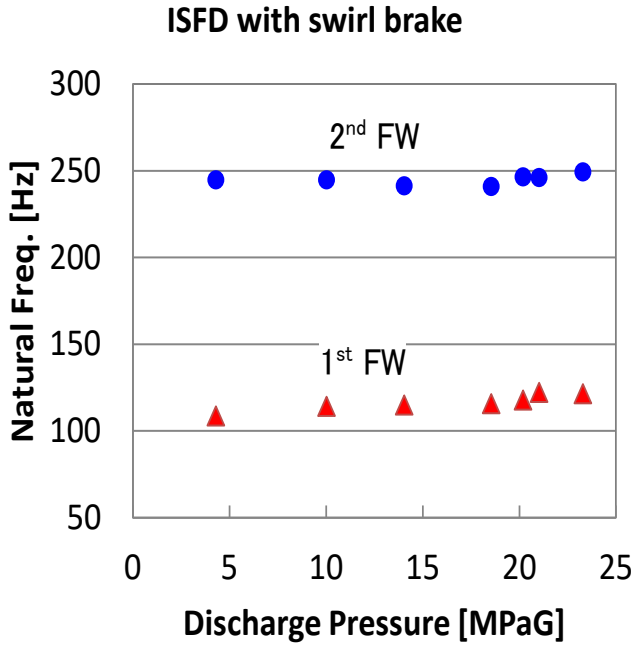

Figure 34: Measured Natural Frequency vs Discharge Pressure (ISFD Bearing)

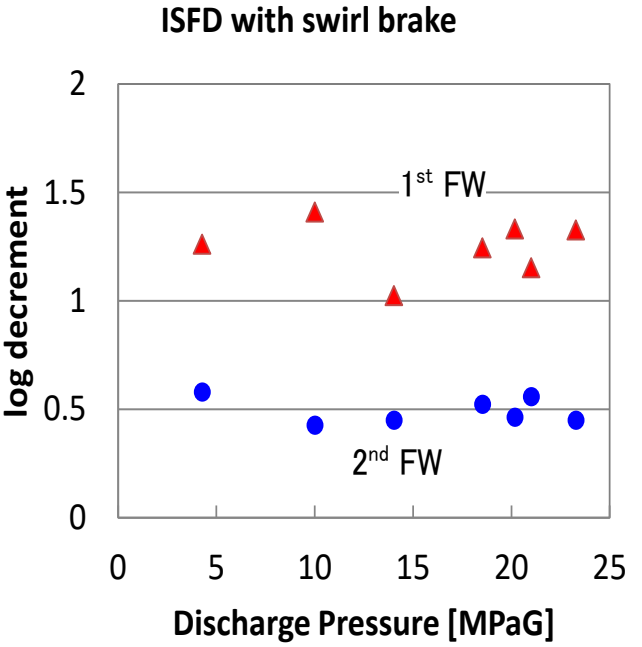

Figure 35: Measured log decrement vs Discharge Pressure (ISFD Bearing)

DYNAMIC BLADE STRESS EVALUATION OF OPEN IMPELLERS USING BLADE VIBRATION MEASUREMENT

Justification of Blade Vibration measurement

The impeller, which is a main part of the centrifugal compressor, is exposed not only to the mean stress due to centrifugal force, but also to dynamic stress caused by compressed gas flow. It is considered that a large dynamic force acts on the impeller especially under high pressure condition, so it is very important to confirm the mechanical strength reliability of the impeller blades in actual compressor operation. The tested compressor has five impellers, in which 7th and 8th stage impellers are covered type, whereas 4th, 5th and 6th stage impellers are open type. The open impeller consists of an axisymmetric disk and blades without an impeller shroud cover, and there is a possibility that large dynamic stress may occur when each blade tip vibrates greatly. Therefore, the blade vibrations of 5th and 6th stage impellers were measured and the dynamic blade stress was evaluated.

Dynamic stress measurement on the blade surface using strain gauges has been conventionally applied to evaluate the mechanical strength reliability of impellers. Although this method can measure the strain directly related to the stress, it is necessary to mount strain gauges with wirings on the blade surfaces and to install signal communication devices such as a telemetry system or a slip ring to a rotating part. Alternatively, there is a blade vibration measurement (BVM, so-called blade tip-timing measurement) method using a non-contact displacement sensor to easily measure the blade vibration behavior. This method has been applied to axial flow type large gas turbines and steam turbines and it doesn`t require installing sensors to the rotating part. The authors have applied BVM method to industrial centrifugal compressors and evaluated the dynamic blade stress. The dynamic blade stress estimated by blade vibration measurement was successfully validated with the data measured simultaneously by strain gauges (Iwata et al 2017).

The BVM system measures blade passing time via non-contact sensors such as optical probes or eddy current probes. Blade vibration amplitudes and frequencies are analyzed based on the deviation of blade passing time per rotation. The non-contact sensors are installed in stationary casing, and their output analog signals of blade tip passing are triggered to generate pulses as shown in Figure 36. When the blade tip oscillates, the time difference between the tip passing timing and non-oscillating pulse signal for shaft rotational speed detection changes, and the blade vibration is analyzed based on the deviation of the passing timing for each rotation. In this measurement, the blade tip passing speed was about 413ft/s / 126 m/s at maximum, and the high-frequency of 80 MHz clock was used for precise timing of the blade passing pulse (i.e., vibration measurement resolution of about 0.06mils / 1.6 um).

As shown in Figure 37, optical non-contact displacement sensors were installed to 5th and 6th stage casings, and the vibration displacement of the impeller blade tips was measured. The vibration of all blades can be measured by BVM system. Six sensors were arranged in a circumferential direction for each impeller to improve the accuracy in analyzing the amplitude and frequency.

When the vibration mode shape of impeller changes, the peak amplitude of dynamic stress and the location where it occurs are different even if the vibration displacement of the blade tip is the same. Therefore, it is important not only to measure tip vibration amplitude, but also to specify the vibration mode. The relationship between displacement and stress in a specific vibratory mode can be obtained by FEM modal analysis as shown in Figure 38. This figure shows the first and second mode shapes of vibration displacement and stress distribution. When the vibration mode shape and the impeller blade tip amplitude can be specified by BVM, it is possible to estimate the dynamic stress using displacement versus stress relationship in the corresponding vibration mode. In order to reduce the estimation error, it is preferable to measure the tip vibration where the amplitude of vibration is the largest.

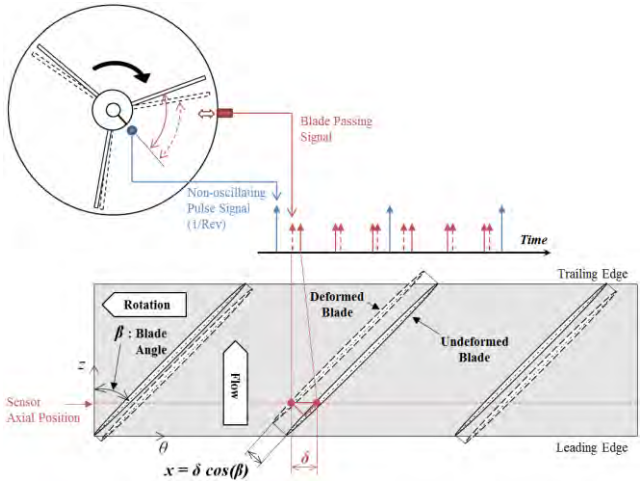

Figure 36: Measurement Principle of Blade Vibration Measurements

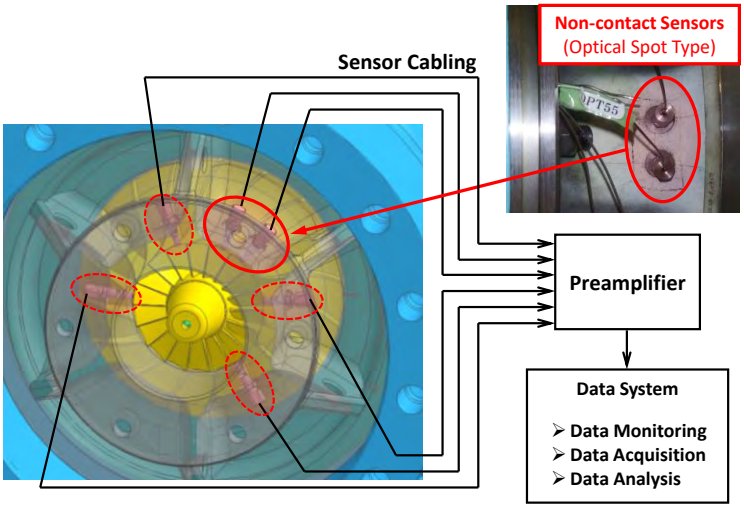

Figure 37: Optical Spot Sensors for Blade Vibration Measurement for 5th stage Impeller

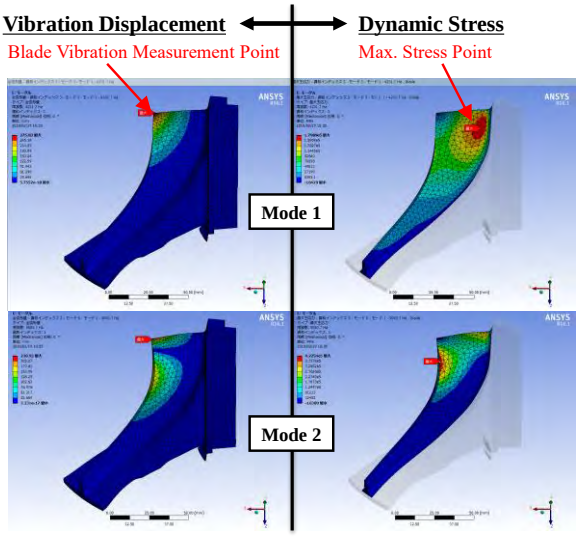

Figure 38: FEM Modal Analysis Result of 5th Stage Impeller

Evaluation of dynamic blade stress at blade resonance

The blade vibration of 5th and 6th stage impellers were measured during startup, coast-down operations under low pressure condition and during deceleration operations under low / medium / high pressure conditions. The discharge pressure at 5th stage during deceleration operation was 30/ 390/ 770 psiA (0.2 / 2.7 / 5.3 MPaA) under low / medium / high pressure conditions, respectively.
Figure 39 shows vibration response of all blades 5th stage impeller during deceleration operations under low pressure condition. BM1 (Blade Mode 1) resonance was observed at around 17500 rpm. The frequency of this resonance was around 4375 Hz, which was 15 times (=diffuser vane number) of rotational speed. Figure 40 shows the blade vibration response under medium pressure operation. BM1 resonance was observed at around 17360rpm. The peak amplitude at medium pressure was observed to be smaller than low pressure and also the peak frequency shifts a bit lower compared with low pressure operation. On the other hand, BM1 resonance was not clearly confirmed at high pressure operation. The maximum dynamic stress at low pressure was estimated to be 3 percent of blade material strength using the measured blade tip amplitudes and FEM results. It was found that the dynamic stress of 5th stage impeller was sufficiently lower compared with material strength. For 6th stage impeller, the response peak was not clearly observed and the natural frequency itself could not be measured under any operating conditions. Therefore, it was confirmed that the blade stress

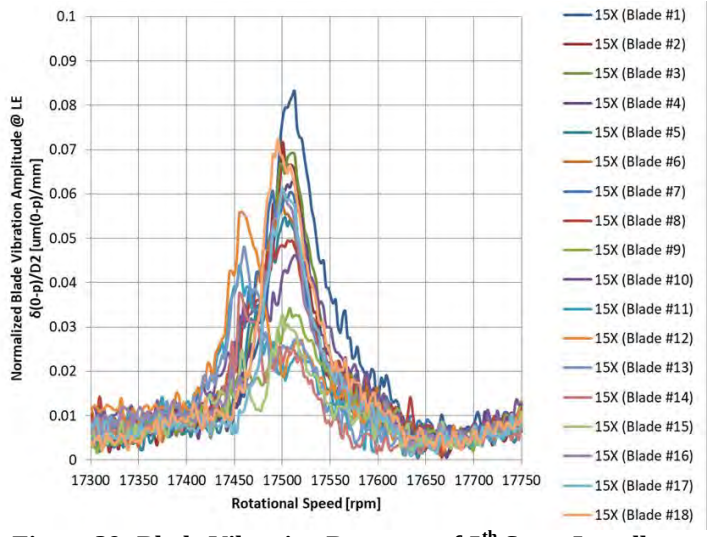

Figure 39: Blade Vibration Response of 5th Stage Impeller under low pressure condition

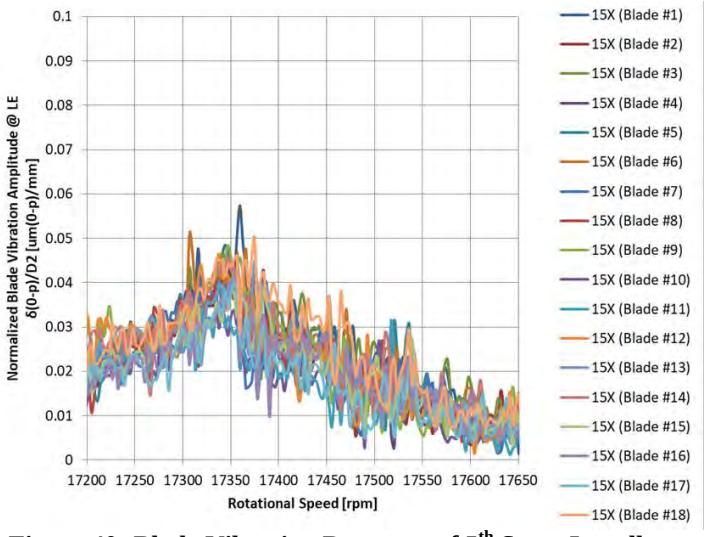

Figure 40: Blade Vibration Response of 5th Stage Impeller under medium pressure condition

at resonance was sufficiently small for 6th stage impeller also. From the above, it was confirmed that the resonance stresses for 5th and 6th stage impellers were sufficiently small.

Evaluation of dynamic blade stress at rated speed

Figure 40 shows compressor performance curves for 5th and 6th stages with circles, and these diameters indicate overall amplitudes of blade vibration normalized by impeller tip diameter D2. The horizontal axis shows the flow coefficient. The discharge pressure and vibration amplitude are shown at various operating conditions. The normalized blade vibration amplitude for 5th and 6th stage impellers was about the same level, and the change due to discharge pressure and flow coefficient was limited. However, the maximum amplitude was observed at minimum flow rate close to the surge line. The maximum amplitude was about 5 times the maximum response at resonance in Figure 38. Asynchronous analysis of the measured vibration was performed. The BM1 mode frequency was observed in some cases, but in most cases there will be no dominant frequency. Since it is difficult to determine the frequency of vibration, the dynamic blade stress could not be evaluated accurately. However, it was estimated by the following procedures. The first method is to assume that all the amplitude consists of BM1 mode and the stress was estimated based on displacement versus stress relationship of BM1 mode.

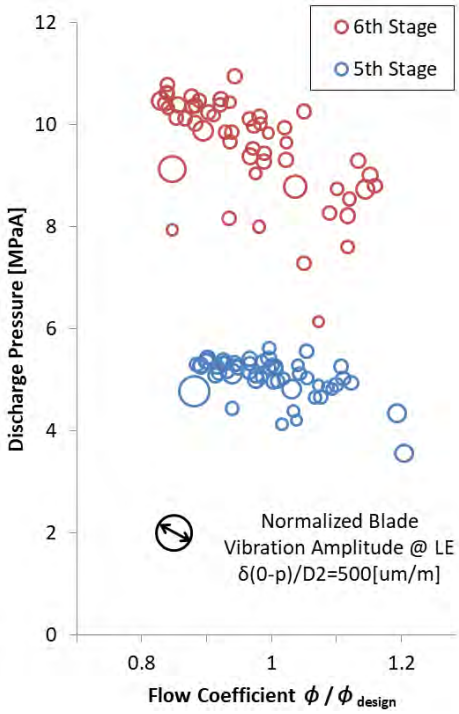

Figure 41: Blade vibration amplitudes of 5th and 6th Stage Impellers

The second is to assume that the BM1, BM2 and BM3 modes appeared equally. The frequency of the BM3 mode is over 13 kHz and it was considered high enough to estimate the dynamic blade stress. The measured blade vibration was divided into each mode component, and the stress of each mode was estimated based on displacement versus stress relationship of each mode, and then added together to obtain the dynamic stress values. The estimated dynamic stress for the first method was 18 percent and the second was 36 percent of the blade material strength. These values were sufficiently low with regard to the material strength.

Summary of dynamic blade stress evaluation

The dynamic blade stress of 5th and 6th stage impellers at various operating conditions was measured. The resonance response of blade stress during startup and coast-down operations was very small compared to the blade material strength. Regarding the rated speed condition, it was difficult to estimate accurate dynamic stress, but roughly estimated stress was sufficiently lower than material strength.

THRUST FORCE MEASUREMENT OF PINION ROTOR

Thrust force measurement method

The thrust force acting on a compressor pinion shaft of changes widely depending on compressor operating conditions. Therefore, it is important to measure the actual thrust forces under various compressor operations and to validate the thrust bearing design. The thrust bearing forces were measured for 5th to 6th stage rotor and 7th to 8th stage rotor. Figure 42 is a photo of thrust bearing with thrust force sensors. Figure 43 shows the thrust bearing pad with strain gauges. The thrust force acting on the pad was measured using these gauges. Four single element strain gauges were attached to the bearing pad web as described in this figure, and these gauges were wired as Wheatstone bridge circuit. The force was obtained by measuring the output voltage of bridge circuit. Three pads with gauges were attached to 5th, 6th, 7th and 8th stage thrust bearings, respectively.
Two loading tests were carried out to verify the measurement accuracy of strain gauges before installing the thrust bearings to the compressor. First, the relationship between compressive load acting on a single pad and output voltage of Wheatstone bridge circuit was measured, and the strain gauge sensor's sensitivities were obtained. Then, the static load test for thrust bearing assemblies was performed, and it was confirmed that the force measurement accuracy of the bearings was within ±12 percent in the tested force range.

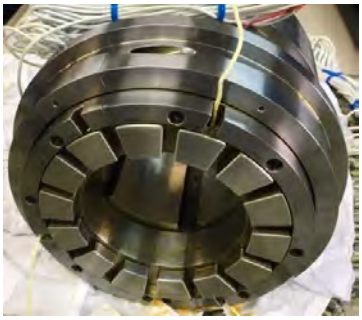

Figure 42: Thrust Bearing with Strain Gauge

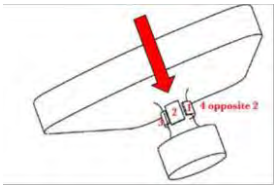

Figure 43: Thrust Pad with Four Strain Gauges

Thrust force measurement result

The bearing thrust force and bearing pad temperature was recorded in a wide operating range. The specification of thrust bearings is mentioned in Table 4. Figure 44 shows the maximum thrust force and maximum pad temperature for 7th and 8th bearings. The authors prepared two dry gas seals for 8th stage with different balance diameters namely DGS1 and DGS2. The balance diameter of DGS1 was larger than that of DGS2. It was observed that, the thrust force measured at 7th stage with DGS2 was larger compared to DGS1. The design value of thrust load was also shown in this figure. The measured maximum thrust force was almost same as design value in case of DGS2 and much lower in case of DGS1. The maximum temperature was 198°F / 92 °C in case of DGS1.The measured maximum thrust force of 5th and 6th bearings were sufficiently lower than the design values and the maximum pad temperature was 187°F / 86 °C throughout all the tests. Acquired data have verified that the thrust bearing design is adequate.

Figure 44: Thrust Force Measurement Result (7th and 8th Stages)

CONCLUSIONS

Comprehensive tests were conducted for the main component as well as the complete machine and experimentally determined not only general performances such as overall aerodynamics and rotor vibrations but also usually unknown parameters. By implementing state-of-the-art techniques, the unknown parameters like rotor natural frequency and log decrement, impeller blade vibratory stress and thrust force on bearings could be accurately measured. The overall performance result met the expectations and the measurements had quantitatively verified the mechanical reliability of compressor. As an outcome of series of experimental evaluations it is concluded that this integrally geared CO2 centrifugal compressor is highly efficient with improved reliability can be used for high pressure applications, which will also contribute to energy saving and global environmental conservation.

NOMENCLATURE

QA	= Anticipated Cross Coupling for the Rotor	(-)
η p	= Polytropic Efficiency	(-)
ϕ	= Flow Coefficient	(-)
FRFs	= Frequency Response Functions	
dFRFs	= Directional Frequency Response Functions	

REFERENCES

API STANDARD 617, SEPTEMBER 2014, "Axial and Centrifugal Compressors and Expander-compressors," EIGHTH EDITION, American Petroleum Institute,, Washington, D.C.

Baldassarre, L., and Masi, G., September 2014, Optimization of Swirl Brake Design And Assessment of Its Stabilizing Effect on Compressor Rotordynamic Performance、Proceedings of 43rd Turbo Machinery Symposium, Houston,2014

Bennett, J., Wilkes, J., and Wygant, K., June 2017, "Cycle Modeling and Optimization of an Integrally Geared sCO2 Compander," Proceedings of ASME Turbo Expo 2017: Turbomachinery Technical Conference and Exposition

Iwata, T., Baba, Y., Saeki, K., Kameyama, Y., Shiga, T., 2017, "Experimental Evaluation of Mechanical Reliability of the Impeller Blade for Large Integrally Geared Compressors," 46th Turbomachinery & 33rd Pump Symposia, Turbomachinery Laboratory, Texas A & M University, College Station, Texas

Kulhanek C. D., Moore J, Lillard J., Nordwall G., Elliott G., Shoup T., 2017, "Eliminating a Rotordynamic Instability of a 12 MW Overhung, Radial Inflow Expander," Proceedings of 46rd Turbomachinery Symposium, Houston

Metz, K., Warkus, C., Schldhauer, M., Hylla, E., "June 2015 CO2 Research Rig for Advanced Compressors (CORA)," Proceedings of ASME Turbo Expo 2015: Turbine Technical Conference and Exposition

Moore, J., Ransom, D., and Viana, F., APRIL 2011, "Rotordynamic Force Prediction of Centrifugal Compressor Impellers Using Computational Fluid Dynamics," Vol. 133, Journal of Engineering for Gas Turbines and Power

Musardo, A., Patel, V., Giovani, G., and Cipriani, S., September 2012, "CO2 Compression at World's Largest Carbon Dioxide Injection Project," Proceedings of the Fortieth Turbomachinery Symposium

Nishida, H., Kobayashi, H., and Fukushima, Y., 1991, "A Study on the Rotating Stall of Centrifugal Compressors (3rd Report, Rotating Stall Suppression Method)," Vol. 57, No.543, Japan Society of Mechanical Engineering

Noronha R. F., Miranda M. A., Cavalca K. L., Memmott E., 2014, "A., "Stability Testing of CO_2 Compressors," Proceedings of 43rd Turbomachinery Symposium, Houston

Takahashi N., Fujiwara H., Matsushita O., Ito M., Fukushima Y., 2007, "An Evaluation of Stability Indices Using Sensitivity Functions for Active Magnetic Bearing Supported High-Speed Rotor," ASME Journal of Vibration and Acoustics, April, Vol. 129

Takahashi N., Narita M., Magara Y., Miura H., 2011, "Rotordynamic Evaluation of Centrifugal Compressor Using Electromagnetic Exciter," GT2011-45829, Proceedings of ASME Turbo Expo 2011, Vancouver, Canada, June 6–10

Tokuyama S., Nakaniwa A., Yoshikazu D., Saburi S., 2014, "Development of a High Pressure Ratio and wide operating range 700bar

compressor," Proceedings of 43rd Turbomachinery Symposium, Houston

Vannini G., Pelagotti A., Rizzo E., Carmicino C., 2017, "Rotordynamic Test Results from a High Flexibility Ratio - High Pressure Fully Instrumented Centrifugal Compressor Test Vehicle," Proceedings of 46rd Turbomachinery Symposium, Houston

Vannini G., Vescovo G. D., Bertoneri M., Wilcox M., 2014, "Centrifugal Compressor Rotordynamics in Wet Gas Conditions," Proceedings of 43rd Turbomachinery Symposium, Houston

ACKNOWLEDGEMENTS

The authors express deep gratitude to Mr. Matsuoka, Mr. Noda and all staff members in the manufacturing section for their utmost effort to accomplish this prototype compressor test. The authors also would like to thanks Mr. Deguchi for supporting the aerodynamic matters of this project as a specialist in fluid dynamics of turbomachinery.